Slovak University of Technology in Bratislava
Institute of Information Engineering, Automation, and Mathematics

PROCEEDINGS

of the 18th International Conference on Process Control

Hotel Titris, Tatranská Lomnica, Slovakia, June 14 – 17, 2011

ISBN 978-80-227-3517-9

http://www.kirp.chtf.stuba.sk/pc11

Editors: M. Fikar and M. Kvasnica

Podmajerský, M., Fikar, M.: Real-time Dynamic Optimisation by Integrated Two-Time-Scale Scheme, Editors: Fikar, M., Kvasnica, M., In *Proceedings of the 18th International Conference on Process Control*, Tatranská Lomnica, Slovakia, 543–551, 2011.

Full paper online: http://www.kirp.chtf.stuba.sk/pc11/data/abstracts/081.html

Real-time Dynamic Optimisation by Integrated Two-Time-Scale Scheme

Marián Podmajerský * **Miroslav Fikar** *

* *Institute of Information Engineering, Automation and Mathematics, STU in Bratislava, Slovakia*
{*marian.podmajersky,miroslav.fikar*}*@stuba.sk*

Abstract: This paper deals with the problem of uncertainties in optimal control of real process. The measurement-based optimisation is used to treat variations in terminal constraints, model mismatch and process disturbances. It is assumed that this process will be carried out several times in a row and so that run-to-run optimisation can be performed. The paper presents an integrated two-time-scale control where constraints in optimisation problem are adopted between runs and the pre-computed optimal inputs are corrected according to the on-line output measurements during the run. Moreover, the proposed control approach has been implemented to control level transition in two connected tanks with liquid interaction. The results uncover better convergence properties with the resulting control scheme than individual schemes dealing either with run-to-run adaptation or with neighbouring extremal corrections inside the run.

Keywords: dynamic optimisation, neighbouring-extremal control, optimal control, integrated control scheme

1. INTRODUCTION

The processes in general are subject to substantial uncertainty during their operation what lowers quality of the performance and quantity along with operational constraint violations. Common sources of uncertainty include measurement noise, inaccurate model, perturbations in initial conditions, and disturbances during a run-time. Model-based and measurement-based optimisation of dynamic processes are established frameworks that have the ability to mitigate the effect of uncertainty on process performance, especially in the presence of constraints (Kadam and Marquardt, 2007).

In current literature, various optimisation techniques can be found that improve process operation and deal with the influence of uncertainty during the process operation. The most straightforward approach is to implement the optimal inputs obtained as off-line solution of dynamic optimisation problem for the process model and then to track the optimal trajectory on-line. However, in reality, the presence of model mismatch shifts the precomputed optimum what requires on-line corrections of the nominal trajectory in order to ensure optimal operation policy. Different strategy, model predictive control (MPC) (Allgöwer and Zheng, 2000; Garcia et al., 1989; Maciejowski, 2002), implements a re-optimisation of the problem and uses the measurements to update the current state of the model. This strategy suffers two important deficiencies: i) the presence of constraints may result in an infeasible solution; ii) the re-optimisations may not be tractable in real-time. Clearly, the time needed to re-optimise the system depends on both the problem complexity and the computing performance. Long computational time may lead to performance loss, or worse constraint violations, especially in processes with fast process dynamic. Some efficient implementations have been proposed by Biegler (2000); Diehl et al. (2002); Cannon et al. (2001). Explicit MPC approach (Bemporad et al., 2002), multi-parametric programming is used to pre-compute off-line all possible control actions for a given range of the state variables. The control inputs are then adjusted by simply selecting the control law that corresponds to the actual state of the process, as given by the latest measurements. Although this method can accommodate fast sampling times, its foremost limitation comes from the curse of dimensionality and from the quality of the linearisations. This currently limits the application of explicit MPC to problems having no more than a few state variables as well as piece-wise linear dynamics.

In the literature, another control strategy that reduces the online computational effort can be found. Neighbouring extremal (NE) control provides fast suboptimal solutions by not re-solving optimisation problem thus it reduce computational expense. This method was introduced in seventies and eighties by Bryson and Ho (1975); Pesch (1989). In neighbouring extremal control an optimum feedback law is applied to compute control corrections for small variations in state vector. The feedback law is derived around nominal control trajectory obtained from offline solution of dynamic optimisation problem. The optimal control problem and the approximation of the solution for perturbed process are subject to boundary value problem. The derivation of the boundary problem is not straightforward and the good initial guess are required to estimate adjoint variables. Further drawback is a suboptimality of the solution as the feedback law is derived for the small variations in states in the neighbourhood of the nominal solution. Also, the neighbouring extremal control exhibits lower performance when applied to very non-linear processes, e.g. chemical processes. Closely related real-time

strategy has been proposed by Kadam and Marquardt (2007) for computation of neighbouring extremal solution using direct optimisation methods. With this strategy neighbouring extremal is computed through sensitivity information of the discretised optimal solution, instead of deriving an optimum feedback law.

This paper presents a two-time-scale approach, whereby a run-to-run adaptation strategy (Bonvin et al., 2006) is implemented at the slow time scale (outer loop) and is integrated with a (constrained) neighbouring extremal controller (Bryson and Ho, 1975) that operates at the fast time scale (inner loop). More specifically, run-to-run adaptation of the terminal constraints (Marchetti et al., 2007) is considered for the outer loop. In its original form, this scheme proceeds by re-optimising the batch operation between each run and adapting the terminal constraints based on the mismatch between their predicted and measured values; but no adaptation is made within a run. In order to reject disturbances within each run and at the same time promote feasibility and optimality, a NE controller is here considered as the inner loop. The NE control which avoids the costly re-optimisation of dynamic systems and approximates the optimal solution of perturbed system, is well-suited for this purpose. The integration between the outer- and inner-loops occurs naturally since the NE controllers are recalculated after each run based on the solution to the outer-loop optimization problem. The resulting integrated two-time-scale optimization scheme thus offers promise to enhance performance and tractability.

The paper is structured as follows. Section 2 defines dynamic optimisation problem and necessary conditions of optimality, Next, Section 3 provides theoretical background on NE control and its numerical computation. Run-to-run constraint optimisation is outlined in Section 4. The proposed integrated two-times-scale optimisation scheme is closely described in Section 5. The performance of the proposed approach is demonstrated on level control of two connected tanks with liquid interaction, in Section 6. Finally, Section 7 concludes the paper.

2. DYNAMIC OPTIMISATION PROBLEM

2.1 Problem Formulation

Throughout the paper, the following dynamic optimisation problem with control and terminal bound constraints is considered:

$$\min_{\boldsymbol{u}} \; J = \phi(\boldsymbol{x}(t_f)) + \int_0^{t_f} L(\boldsymbol{x}(t), \boldsymbol{u}(t))\mathrm{d}t \tag{1}$$

$$\text{s.t.} \quad \dot{\boldsymbol{x}} = \boldsymbol{F}(\boldsymbol{x}(t), \boldsymbol{u}(t)), \quad 0 \le t \le t_f \tag{2}$$

$$\boldsymbol{x}(0) = \boldsymbol{x}_0 \tag{3}$$

$$\boldsymbol{\psi}(\boldsymbol{x}(t_f), t_f) \le \boldsymbol{\psi}_{ref} \tag{4}$$

$$\boldsymbol{u}^L \le \boldsymbol{u}(t) \le \boldsymbol{u}_U. \tag{5}$$

In (1)–(5), $t \ge 0$ denotes the time variable, with t_f the final time; $\boldsymbol{u} \in \mathbb{R}^{n_u}$ the control vector; $\boldsymbol{x} \in \mathbb{R}^{n_x}$ the state vector, with initial value $\boldsymbol{x}_0$; J, ϕ and L the scalar cost, terminal cost, and integral cost, respectively; and $\boldsymbol{\psi}$ the vector of n_ψ terminal constraints. All the functions in (1)–(5) are assumed to be continuously differentiable with respect to all their arguments.

2.2 Necessary Conditions for Optimality

Following Bryson and Ho (1975), the Hamiltonian function H is defined as follows:

$$H(\boldsymbol{x}, \boldsymbol{u}, \boldsymbol{\lambda}, \boldsymbol{\mu}^L, \boldsymbol{\mu}^U) = L(\boldsymbol{x}, \boldsymbol{u}) + \boldsymbol{F}(\boldsymbol{x}, \boldsymbol{u})^T \boldsymbol{\lambda} + \tag{6}$$

$$+ \boldsymbol{\mu}^L(\boldsymbol{u}^L - \boldsymbol{u}) + \boldsymbol{\mu}^U(\boldsymbol{u} - \boldsymbol{u}^U), \tag{7}$$

$\boldsymbol{\lambda} \in \mathbb{R}^{n_x}$ denotes the so-called adjoint (or costate) vector which satisfies

$$\dot{\boldsymbol{\lambda}} = -\boldsymbol{H}_{\boldsymbol{x}} = -\boldsymbol{F}_{\boldsymbol{x}}^T \boldsymbol{\lambda} - \boldsymbol{L}_{\boldsymbol{x}}, \; 0 \le t \le t_f, \tag{8}$$

with the terminal conditions given by

$$\boldsymbol{\lambda}(t_f) = \left[\boldsymbol{\phi}_{\boldsymbol{x}} + \boldsymbol{\nu}^T \boldsymbol{\psi}_{\boldsymbol{x}}\right]_{t=t_f}, \tag{9}$$

$\boldsymbol{\mu}^L(t), \boldsymbol{\mu}^U(t) \in \mathbb{R}^{n_u}$ are Lagrange multiplier vector functions satisfying

$$\boldsymbol{\mu}^{L^T}(\boldsymbol{u}^L - \boldsymbol{u}) = \boldsymbol{0}; \quad \boldsymbol{\mu}^L \ge \boldsymbol{0} \tag{10}$$

$$\boldsymbol{\mu}^{U^T}(\boldsymbol{u} - \boldsymbol{u}^U) = \boldsymbol{0}; \quad \boldsymbol{\mu}^U \ge \boldsymbol{0}, \quad 0 \le t \le t_f. \tag{11}$$

and $\boldsymbol{\nu} \in \mathbb{R}^{n_\psi}$ are Lagrange multipliers for the terminal constraints such that

$$\boldsymbol{0} = \nu_k \psi_k, \quad \nu_k \ge 0, \quad \text{for each } k = 1, \ldots, n_\psi. \tag{12}$$

Provided that the optimal control problem is not abnormal, the first- and second- order necessary conditions for optimality (NCO) read:

$$H_{\boldsymbol{u}} = L_{\boldsymbol{u}} + \boldsymbol{F}_{\boldsymbol{u}}^T \boldsymbol{\lambda} - \boldsymbol{\mu}^L - \boldsymbol{\mu}^U = \boldsymbol{0} \tag{13}$$

$$H_{\boldsymbol{uu}} \ge 0 \tag{14}$$

This latter determines the set of active terminal constraints at the optimum, which is denoted by the vector $\bar{\boldsymbol{\psi}}$ of dimension $n_{\bar{\psi}}$ and by complementary multiplier $\bar{\boldsymbol{\nu}}^*$. The constraints are inactive when the crresponding Lagrange multiplier is equal to zero. (The subscript such as $_y$ for a given variable denotes partial derivatives of that variable with respect to y.)

3. NEIGHBOURING-EXTREMAL CONTROL

3.1 Neighbouring Control

Let's assume that the optimal control trajectory $\boldsymbol{u}^*(t)$ for the optimisation problem (1)–(5) consists of a sequence of constrained and unconstrained arcs. The optimal solution then comprises $\boldsymbol{x}^*(t)$, $\boldsymbol{\lambda}^*(t), \bar{\boldsymbol{\nu}}^*, \boldsymbol{\mu}^L, \boldsymbol{\mu}^U, 0 \le t \le t_f$. For the control sequence, it is also assumed that the uncertainty is sufficiently small for the perturbed optimal control to have the same sequence of constrained and unconstrained arcs as the nominal solution.

The constrained optimal control problem obtained with a small variation in the initial condition $\boldsymbol{x}(0) = \boldsymbol{x}_0 + \delta\boldsymbol{x}_0$ and in active terminal constraints $\bar{\boldsymbol{\psi}}(\boldsymbol{x}(t_f), t_f) = \delta\bar{\boldsymbol{\psi}}$ produces variations in optimal control vector $\delta\boldsymbol{u}(t)$, state vector $\delta\boldsymbol{x}(t)$, adjoint vector $\delta\boldsymbol{\lambda}(t)$ and Lagrange multiplier vector $\delta\bar{\boldsymbol{\nu}}$ (for the active terminal constraints $\bar{\boldsymbol{\psi}}$). Along unconstrained arcs, these variations can be calculated from the linearisation of the first-order NCO (10)–(12) around the extremal path (Bryson and Ho, 1975):

$$\delta\dot{\boldsymbol{x}} = \boldsymbol{F}_{\boldsymbol{x}}^* \delta\boldsymbol{x} + \boldsymbol{F}_{\boldsymbol{u}}^* \delta\boldsymbol{u} \tag{15}$$

$$\delta\dot{\boldsymbol{\lambda}} = -\boldsymbol{H}_{\boldsymbol{xx}}^* \delta\boldsymbol{x} - \boldsymbol{F}_{\boldsymbol{x}}^{*T} \delta\boldsymbol{\lambda} - \boldsymbol{H}_{\boldsymbol{xu}}^* \delta\boldsymbol{u} \tag{16}$$

$$\boldsymbol{0} = \boldsymbol{H}_{\boldsymbol{ux}}^* \delta\boldsymbol{x} + \boldsymbol{F}_{\boldsymbol{u}}^{*T} \delta\boldsymbol{\lambda} + \boldsymbol{H}_{\boldsymbol{uu}}^* \delta\boldsymbol{u} \tag{17}$$

$$\delta\boldsymbol{x}(0) = \delta\boldsymbol{x}_0 \tag{18}$$

with additional conditions:

$$\delta\boldsymbol{\lambda}(t_f) = \left[\left(\boldsymbol{\phi}^*_{\boldsymbol{xx}} + \bar{\boldsymbol{\nu}}^{*T}\bar{\boldsymbol{\psi}}^*_{\boldsymbol{xx}}\right)\delta\boldsymbol{x} + \bar{\boldsymbol{\psi}}^{*T}_{\boldsymbol{x}}\delta\bar{\boldsymbol{\nu}}\right]_{t=t_f} \quad (19)$$

$$\delta\bar{\boldsymbol{\psi}} = \left[\bar{\boldsymbol{\psi}}^*_{\boldsymbol{x}}\delta\boldsymbol{x}\right]_{t=t_f}. \quad (20)$$

A superscript * indicates that the corresponding quantity is evaluated along the extremal path $\boldsymbol{u}^*(t)$, $0 \le t \le t_f$, and corresponding states, adjoints and Lagrange multipliers.

Let us assume that the Hamiltonian function is regular, so that $\boldsymbol{H}^*_{\boldsymbol{uu}}$ is invertible along $0 \le t \le t_f$. The control variation $\delta\boldsymbol{u}(t)$ for these unconstrained arcs $\boldsymbol{\mu}^L = \boldsymbol{\mu}^U = \boldsymbol{0}$ is then given from (17):

$$\delta\boldsymbol{u}(t) = -(\boldsymbol{H}^*_{\boldsymbol{uu}})^{-1}\left[\boldsymbol{F}^{*T}_{\boldsymbol{u}}\delta\boldsymbol{\lambda}(t) + \boldsymbol{H}^*_{\boldsymbol{ux}}\delta\boldsymbol{x}(t)\right]. \quad (21)$$

Overall, along constrained arcs, the control variation is equal to zero $\delta\boldsymbol{u}(t) = 0$. Then, $\delta\boldsymbol{x}(t)$ and $\delta\boldsymbol{\lambda}(t)$ satisfy the following multi-point boundary value problem (MPBVP):

$$\begin{pmatrix}\delta\dot{\boldsymbol{x}}(t)\\ \delta\dot{\boldsymbol{\lambda}}(t)\end{pmatrix} = \boldsymbol{\Delta}(t)\begin{pmatrix}\delta\boldsymbol{x}(t)\\ \delta\boldsymbol{\lambda}(t)\end{pmatrix},$$

$$\delta\boldsymbol{x}(0) = \delta\boldsymbol{x}_0, \quad \delta\bar{\boldsymbol{\psi}} = \left[\bar{\boldsymbol{\psi}}^*_{\boldsymbol{x}}\delta\boldsymbol{x}\right]_{t=t_f},$$

$$\delta\boldsymbol{\lambda}(t_f) = \left[\left(\boldsymbol{\phi}^*_{\boldsymbol{xx}} + \bar{\boldsymbol{\nu}}^{*T}\bar{\boldsymbol{\psi}}^*_{\boldsymbol{xx}}\right)\delta\boldsymbol{x} + \bar{\boldsymbol{\psi}}^{*T}_{\boldsymbol{x}}\delta\bar{\boldsymbol{\nu}}\right]_{t=t_f} \quad (22)$$

where:

$$\boldsymbol{\Delta}(t) = \begin{cases}\begin{pmatrix}\boldsymbol{\alpha}(t) & -\boldsymbol{\beta}(t)\\ -\boldsymbol{\gamma}(t) & -\boldsymbol{\alpha}(t)^T\end{pmatrix} & \text{along unconstrained arcs}\\ \begin{pmatrix}\boldsymbol{F}^*_{\boldsymbol{x}} & \boldsymbol{0}\\ -\boldsymbol{H}^*_{\boldsymbol{xx}} & -\boldsymbol{F}^{*T}_{\boldsymbol{x}}\end{pmatrix} & \text{along constrained arcs}\end{cases} \quad (23)$$

and

$$\boldsymbol{\alpha}(t) := \boldsymbol{F}^*_{\boldsymbol{x}} - \boldsymbol{F}^*_{\boldsymbol{u}}(\boldsymbol{H}^*_{\boldsymbol{uu}})^{-1}\boldsymbol{H}^*_{\boldsymbol{ux}} \quad (24)$$

$$\boldsymbol{\beta}(t) := \boldsymbol{F}^*_{\boldsymbol{u}}(\boldsymbol{H}^*_{\boldsymbol{uu}})^{-1}\boldsymbol{F}^{*T}_{\boldsymbol{u}} \quad (25)$$

$$\boldsymbol{\gamma}(t) := \boldsymbol{H}^*_{\boldsymbol{xx}} - \boldsymbol{H}^*_{\boldsymbol{xu}}(\boldsymbol{H}^*_{\boldsymbol{uu}})^{-1}\boldsymbol{H}^*_{\boldsymbol{ux}}. \quad (26)$$

Clearly, at each switching point between an unconstrained and a constrained arcs, a continuity of control, state and adjoint profiles must be preserved. For example, at a switching point between a lower bound and an interior arc, the value of control on lower bound matches the value of control in the interior arc $\boldsymbol{u}^H = \boldsymbol{u}^L$. Here, $\boldsymbol{u}^H$ represents the control obtained from solving the condition $H_{\boldsymbol{u}} = 0$. In addition, state and adjoint trajectories are continuous at this point, too:

$$\boldsymbol{x}^*(t_k^+) = \boldsymbol{x}^*(t_k^-), \quad \boldsymbol{\lambda}^*(t_k^+) = \boldsymbol{\lambda}^*(t_k^-) \quad (27)$$

Variations in switching times are difficult to determine and complicate the calculation of the NE control. To make this implementable, it is considered that the switching points are constant at their nominal times. The control values are then updated only between the fixed times. In practice, performance loss is negligible for small variations of switching times.

3.2 Numerical Computation of Neighbouring Feedback Control

The linear MPBVP (22) can be used to calculate the neighboring-extremal control correction $\delta\boldsymbol{u}(t)$, $0 \le t \le t_f$, in either one of two situations:

i. The initial state and (active) terminal constraint variations $\delta\boldsymbol{x}_0$ and $\delta\bar{\boldsymbol{\psi}}$ are available at discrete time instants, in which case the discrete feedback control can be obtained by directly re-solving the MPBVP. This can be done via a shooting method as described in Pesch (1989);
ii. The variations $\delta\boldsymbol{x}_0$ and $\delta\bar{\boldsymbol{\psi}}$ are available continuously in time, in which case the backward sweep method (Bryson and Ho, 1975) can be used to derive an explicit feedback control law. This approach is closely explained by Bryson and Ho (1975).

In this paper, we consider the first approach that is summarised in Subsection 3.3.

3.3 Shooting Method

The linear TPBVP (22) can be rewritten in the form

$$\begin{pmatrix}\delta\dot{\boldsymbol{x}}(t)\\ \delta\dot{\boldsymbol{\lambda}}(t)\end{pmatrix} = \underbrace{\begin{pmatrix}\boldsymbol{\alpha}(t) & \boldsymbol{\beta}(t)\\ -\boldsymbol{\gamma}(t) & -\boldsymbol{\alpha}(t)\end{pmatrix}}_{=:\,\boldsymbol{\Delta}(t)}\begin{pmatrix}\delta\boldsymbol{x}(t)\\ \delta\boldsymbol{\lambda}(t)\end{pmatrix}, \quad (28)$$

with the boundary conditions

$$\begin{pmatrix}\boldsymbol{I} & \boldsymbol{0}\\ \boldsymbol{0} & \boldsymbol{0}\end{pmatrix}\begin{pmatrix}\delta\boldsymbol{x}(0)\\ \delta\boldsymbol{\lambda}(0)\end{pmatrix} + \begin{pmatrix}\boldsymbol{0} & \boldsymbol{0}\\ \boldsymbol{B}_1 & \boldsymbol{I}\end{pmatrix}\begin{pmatrix}\delta\boldsymbol{x}(t_f)\\ \delta\boldsymbol{\lambda}(t_f)\end{pmatrix} = \begin{pmatrix}\delta\boldsymbol{x}_0\\ \boldsymbol{B}_2\end{pmatrix}, \quad (29)$$

where

$$\begin{aligned}\boldsymbol{B}_1 &= -\left[\boldsymbol{\phi}^*_{\boldsymbol{xx}} + \bar{\boldsymbol{\nu}}^{*T}\bar{\boldsymbol{\psi}}^*_{\boldsymbol{xx}}\right]_{t_f}\\ \boldsymbol{B}_2 &= \left[\bar{\boldsymbol{\psi}}^{*T}_{\boldsymbol{x}}\right]_{t_f}\delta\bar{\boldsymbol{\nu}}\end{aligned} \quad (30)$$

The shooting approach proceeds by guessing the missing initial (or terminal) conditions in (29), and adjusting them in such a way that the corresponding terminal (or initial) conditions are satisfied (see, e.g., Pesch, 1989). Given the guess $\delta\boldsymbol{\lambda}(0) = \delta\boldsymbol{\lambda}_0$ for the adjoint variations at initial time $t = 0$, the (unique) solution to the linear ODE system (28) is of the form:

$$\begin{pmatrix}\delta\dot{\boldsymbol{x}}(t;\delta\boldsymbol{\lambda}_0)\\ \delta\dot{\boldsymbol{\lambda}}(t;\delta\boldsymbol{\lambda}_0)\end{pmatrix} = \underbrace{\begin{pmatrix}\boldsymbol{\Upsilon}_1(t;0) & \boldsymbol{\Upsilon}_2(t;0)\\ \boldsymbol{\Upsilon}_3(t;0) & \boldsymbol{\Upsilon}_4(t;0)\end{pmatrix}}_{=:\,\boldsymbol{\Upsilon}(t;0)}\begin{pmatrix}\delta\boldsymbol{x}_0\\ \delta\boldsymbol{\lambda}_0\end{pmatrix}, \quad (31)$$

where the transition matrix $\boldsymbol{\Upsilon}(t;0)$ is obtained as the solution to the initial value problem

$$\frac{\partial}{\partial t}\boldsymbol{\Upsilon}(t;0) = \boldsymbol{\Delta}(t)\boldsymbol{\Upsilon}(t;0),\ 0 \le t \le t_f; \quad \boldsymbol{\Upsilon}(0;0) = \boldsymbol{I}. \quad (32)$$

Substituting (31) into (29) and (20) leads to the following linear system in the variables $\delta\boldsymbol{\lambda}(0), \delta\bar{\boldsymbol{\nu}}$:

$$\begin{pmatrix}\boldsymbol{Z}_1 & \boldsymbol{Z}_2\\ \boldsymbol{Z}_3 & \boldsymbol{0}\end{pmatrix}\begin{pmatrix}\delta\boldsymbol{\lambda}(0)\\ \delta\bar{\boldsymbol{\nu}}\end{pmatrix} = \begin{pmatrix}\boldsymbol{0}\\ \boldsymbol{I}\end{pmatrix}\delta\bar{\boldsymbol{\psi}} - \begin{pmatrix}\boldsymbol{Z}_4\\ \boldsymbol{Z}_5\end{pmatrix}\delta\boldsymbol{x}_0, \quad (33)$$

where

$$\begin{aligned}\boldsymbol{Z}_1 &= \left[\boldsymbol{\phi}^*_{\boldsymbol{xx}} + \bar{\boldsymbol{\nu}}^{*T}\bar{\boldsymbol{\psi}}^*_{\boldsymbol{xx}}\right]_{t_f}\boldsymbol{\Upsilon}_2(t_f;0) - \boldsymbol{\Upsilon}_4(t_f;0)\\ \boldsymbol{Z}_2 &= \left[\bar{\boldsymbol{\psi}}^{*T}_{\boldsymbol{x}}\right]_{t_f}\\ \boldsymbol{Z}_3 &= \left[\bar{\boldsymbol{\psi}}^*_{\boldsymbol{x}}\right]_{t_f}\boldsymbol{\Upsilon}_2(t_f;0)\\ \boldsymbol{Z}_4 &= \left[\boldsymbol{\phi}^*_{\boldsymbol{xx}} + \bar{\boldsymbol{\nu}}^{*T}\bar{\boldsymbol{\psi}}^*_{\boldsymbol{xx}}\right]_{t_f}\boldsymbol{\Upsilon}_1(t_f;0) - \boldsymbol{\Upsilon}_3(t_f;0)\\ \boldsymbol{Z}_5 &= \left[\bar{\boldsymbol{\psi}}^*_{\boldsymbol{x}}\right]_{t_f}\boldsymbol{\Upsilon}_1(t_f;0)\end{aligned} \quad (34)$$

For given initial state and active terminal constraint variations $\delta\boldsymbol{x}_0$ and $\delta\bar{\boldsymbol{\psi}}$, the solution to the linear system (33) provides the corresponding initial adjoint and Lagrange

multiplier variations $\delta\boldsymbol{\lambda}(0)$ and $\delta\bar{\boldsymbol{\nu}}$. Finally, the NE control variation can be calculated from (21) as

$$\delta\boldsymbol{u}(t) = -(\boldsymbol{H}^*_{\boldsymbol{uu}})^{-1}\left(\boldsymbol{H}^*_{\boldsymbol{ux}}\ \boldsymbol{F}^{*T}_{\boldsymbol{u}}\right)\boldsymbol{\Upsilon}(t;0)\begin{pmatrix}\delta\boldsymbol{x}_0\\ \delta\boldsymbol{\lambda}(0)\end{pmatrix}. \quad (35)$$

4. RUN-TO-RUN CONSTRAINT ADAPTATION

The principle behind run-to-run optimization is similar to MPC. But instead of adapting the initial conditions and moving the control horizon as is done in MPC, the adaptation is performed on the optimization model (e.g., model parameters or constraint biases) before re-running the optimizer. In run-to-run constraint adaptation, more specifically, the terminal constraints (4) in the optimization model are adapted after each run as (Marchetti et al., 2007):

$$\boldsymbol{\psi}(\boldsymbol{x}(t_f), t_f) \leq \delta\boldsymbol{\psi}, \quad (36)$$

where $\delta\boldsymbol{\psi}$ stands for the terminal constraint bias. Such a bias can be directly updated as the difference between the available terminal constraint measurements, $\boldsymbol{\psi}^{\text{meas}}$, at the end of each run and the predicted constraint values. This simple strategy may however lead to excessive correction when operating far away from the optimum, and it may also exacerbate the sensitivity of the adaptation scheme to measurement noise. A better strategy consists of filtering the bias, e.g., with a first-order exponential filter:

$$\delta\boldsymbol{\psi}_{k+1} = [\boldsymbol{I} - \boldsymbol{W}]\,\delta\boldsymbol{\psi}_k + \\ + \boldsymbol{W}\left[\boldsymbol{\psi}^{\text{meas}}_k - \boldsymbol{\psi}(\boldsymbol{x}_k(t_f), t_f)\right], \quad (37)$$

with k the run index, and $\boldsymbol{W}$ a gain matrix—typically, a diagonal matrix.

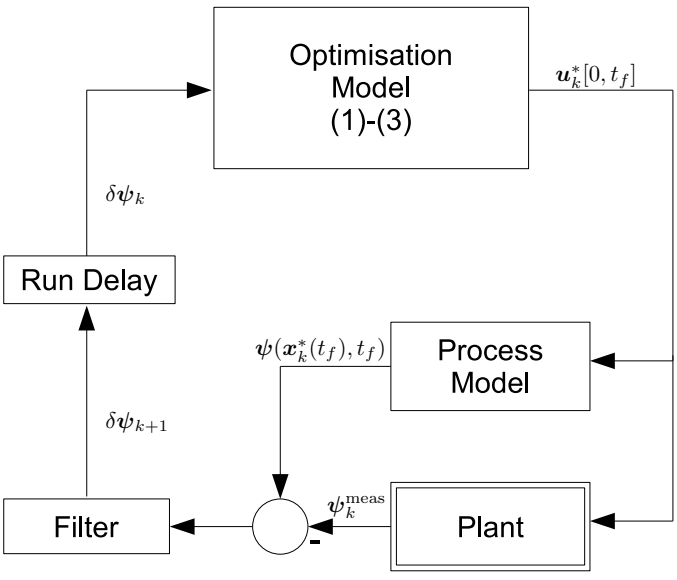

Fig. 1. Run-to-run constraint adaptation scheme.

The run-to-run constraint-adaptation scheme is shown in Figure 1. The constrained dynamic optimisation problem uses the available nominal process model. It is solved between each run, using any numerical procedure, such as the sequential or the simultaneous approach of dynamic optimisation. The optimal control trajectory $\boldsymbol{u}^*_k(t)$, $0 \leq t \leq t_f$, is computed and applied to the plant during the kth run. The predicted optimal response is denoted by $\boldsymbol{x}^*_k(t)$. The discrepancy between the measured terminal constraint values $\boldsymbol{\psi}^{\text{meas}}_k$ and the optimizer predictions $\boldsymbol{\psi}(\boldsymbol{x}^*_k(t_f), t_f)$ is then used to adjust the constraint bias as described earlier, before re-running the optimizer for the next run.

Of course, optimal control trajectory calculated between runs is suboptimal as the real process is never known perfectly.

5. TWO-TIMES-SCALE OPTIMISATION SCHEME

Run-to-run constraint adaptation was shown to be a promising technology in Marchetti et al. (2007). This approach provides a natural framework for handling changes in active constraints in dynamic process systems and it is quite robust towards model mismatch and process disturbances. Moreover, its implementation is simple. Inherent limitations of this scheme, however, are that (i) it does not perform any control corrections during the runs, and (ii) it typically leads to suboptimal performance.

On the other hand, neighbouring-extremal control is able to correct small deviations around the nominal extremal path in order to deliver similar performance as with re-optimisation. Since no costly on-line re-optimisation is needed, this approach is especially suited for processes with fast dynamics. However, the performance of NE control typically decreases dramatically in the presence of large model mismatch and process disturbances, and it requires a full-state measurement. This leads to sub-optimality or, worse, infeasibility when constraints are present or limited measurements are available.

Our proposal is to combine the advantages of these two approaches: Run-to-run constraint adaptation is applied at a slow time scale (outer loop) to handle large model mismatch and changes in active constraints, based on run-end measurements only. Further, NE control is applied at a fast time scale (inner loop) and uses measurement information available within each run, in order to enhance convergence speed and mitigate sub-optimality. It need to be stated that full-state measurement is required even in case of integrated scheme. The proposed integrated two-time-scale optimization scheme is depicted in Figure 2.

The implementation procedure is as follows:

Initialisation:

(0) Initialise the constraint bias $\delta\boldsymbol{\psi} = \boldsymbol{0}$, select a gain matrix $\boldsymbol{W}$ and set the run index to $k = 1$

Outer Loop:

(1) Determine $\boldsymbol{u}^*_k$ by solving the optimal control problem (1)–(5), then obtain the corresponding states $\boldsymbol{x}^*_k$ and adjoints $\boldsymbol{\lambda}^*_k$, with the active terminal constraints $\bar{\boldsymbol{\psi}}$ and Lagrange multipliers $\bar{\boldsymbol{\nu}}^*_k$, and together with Lagrange multipliers for boundary constraints $\boldsymbol{\mu}^L$ and $\boldsymbol{\mu}^U$ that satisfy NCO (10)–(13).

(2) Design a NE controller around the extremal path $\boldsymbol{u}^*_k$, either by using the backward sweep approach (continuous measurements), or by applying the shooting method (discrete measurements).

(3) **Inner Loop:**
Implement the NE controller during the kth run in order to calculate the corrections $\delta\boldsymbol{u}_k(t)$ to $\boldsymbol{u}^*_k(t)$ based on the available (continuous or discrete) process measurements.

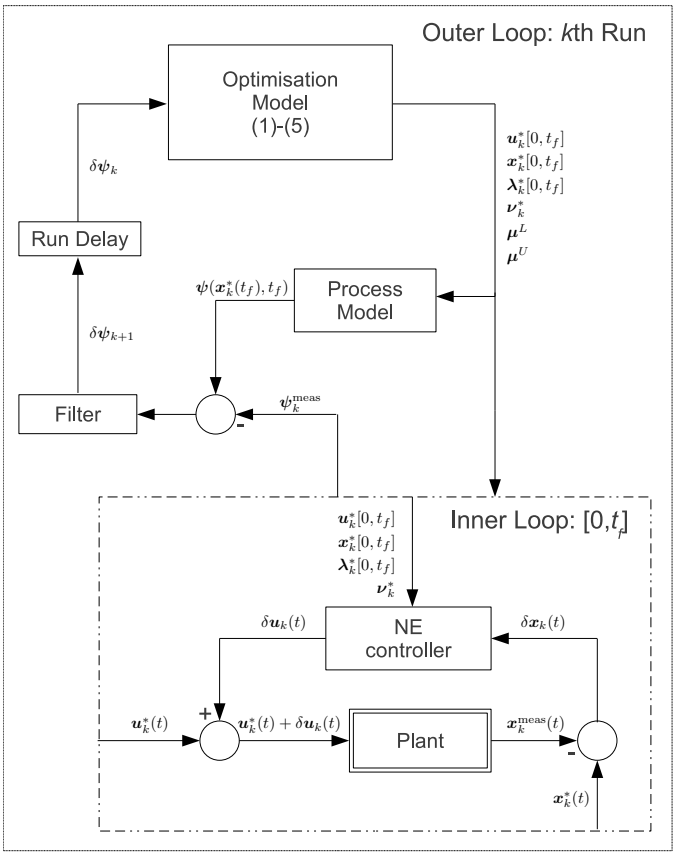

Fig. 2. Two-times-scale optimisation scheme employing NE control in the inner loop and run-to-run constraint adaptation in the outer loop.

(4) Update the constraint bias $\delta\boldsymbol{\psi}_{k+1}$ as the filtered difference between the measured values of the terminal constraints and their predicted counterparts.
(5) Increment the run index $k \leftarrow k+1$, and return to Step 1.

6. TWO CONNECTED TANKS WITH LIQUID INTERACTION

The case study compares the performance of the two-time-scale integrated solution with a pure constraint adaptation control scheme and a pure neighbouring-extremal controller. At first, these control methods are tested in simulations and then they are verified in experimental conditions. The process and its model is introduced next.

6.1 Process Description

Level control of two connected tanks with liquid interaction is considered to illustrate integrated two-times-scale approach as can be seen in Figure 4. The experiment has been carried out on Amira DTS200 device (see Figure 3). There are 3 connected tube-shaped tanks connected through the bottoms and six valves to regulate the outflows. The levels are measured by pressure sensors situated at the bottom of tanks. Also, two inlet flows are available: the first pumps liquid to the first tank and the second pumps liquid to the third tank.

For our purposes, only the first two tanks have been used. The objective is to control level transition from an initial level to the terminal level given for the second tank. The manipulated variable is an inlet flow $u(t)$ pumped into the first tank at the top. The levels $h_1(t)$ and $h_2(t)$ are controlled and measured variables. The measurements are provided by pressure sensors. The outflow is situated at the bottom of the second tank and it is regulated by half-opened valve. Also, a liquid interaction take place, as the tanks are connected through the bottoms.

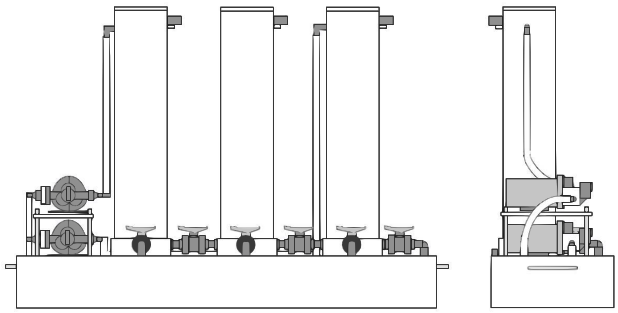

Fig. 3. **Amira DTS200** – Process for level control of tanks.

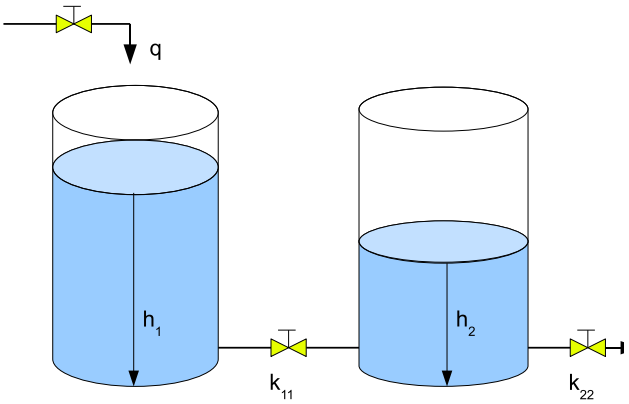

Fig. 4. Configuration of two tanks connected in series.

6.2 Process Model

The model is derived based on the process introduced in the previous subsection. In the model, it is assumed that a liquid density is constant and the walls of tank are vertical to the base. From material balance and from Bernoulli's equation in fluid dynamic, the resulting optimisation problem can be mathematically postulated as follows:

$$\min_u J = \int_{t_0}^{t_f} q(h_2 - h_{2,ref})^2 + ru^2 \mathrm{d}t \tag{38}$$

s.t.

$$\dot{h}_1(t) = \frac{u}{F_1} - \frac{k_{11}}{F_1}\sqrt{h_1 - h_2} \tag{39}$$

$$\dot{h}_2(t) = \frac{k_{11}}{F_2}\sqrt{h_1 - h_2} - \frac{k_{22}}{F_2}\sqrt{h_2} \tag{40}$$

$$\tag{41}$$

The state values $h_1(t)$ and $h_2(t)$ are levels [cm] in the first tank and in the second tank, respectively; constants F_1 and F_2 defines cross-sectional area of tank bases [cm^2]; k_{11} and

k_{22} are valve constants $[\mathrm{cm}^{2.5}\,\mathrm{s}^{-1}]$; variable u represents inlet flow $[\mathrm{ml}\,\mathrm{s}^{-1}]$.

The initial level values are determined at constant inlet flow $u = 25\,\mathrm{ml}\,\mathrm{s}^{-1}$ as $h_1(t) = 16\,\mathrm{cm}$ and $h_2(t) = 8\,\mathrm{cm}$. The numerical values of constants are: cross-sectional areas $F_1 = 154\,\mathrm{cm}^2$ and $F_2 = 154\,\mathrm{cm}^2$; estimated values of valve constants $k_{11} = 10.68\,\mathrm{cm}^{2.5}\,\mathrm{s}^{-1}$ and $k_{22} = 7.5\,\mathrm{cm}^{2.5}\,\mathrm{s}^{-1}$. The final time is set to $t_f = 500\,\mathrm{s}$ and inlet flow u is bounded as:

$$0 \leq u \leq 100\,[\mathrm{ml}\,\mathrm{s}^{-1}]. \tag{42}$$

Desired level in the second tank is $h_{2,ref} = 25\,\mathrm{cm}$, so the additional terminal conditions read:

$$h_2(t_f) = h_{2,ref} \tag{43}$$

$$\dot{h}_1(t_f) = 0 \tag{44}$$

$$\dot{h}_2(t_f) = 0. \tag{45}$$

Note that the integral term $\int_{t_0}^{t_f} ru^2 \mathrm{d}t$ augments the original objective function in order to make the control problem non-singular. Weighting variable r is set as low as possible in order to retain the original objective. This way $H_{\boldsymbol{u}}$ depends on the control variable and Hamiltonian H is regular.

6.3 Nominal Solution

Solving the optimisation problem (38)–(45) with the sequential method (Edgar and Himmelblau, 1988; Guntern et al., 1998), the piecewise constant control profile shows the presence of one interior arc and two boundary arcs. Further analysis of this solution indicates that optimal control consists of a upper bound, lower bound, and an interior constant arc. As the problem is regular, the control action along interior arc can be explicitly determined from the necessary conditions of optimality. Note that along boundary arcs, the control action is determined by an upper or a lower bound hence the control variations are simply $\delta\boldsymbol{u} = 0$. The switching times t_1 and t_2 between these arcs are not explicitly known and they need to be estimated, too. The switching times from piecewise constant control profile give good initial guess for these switching times. Overall, the optimal control solution is given as:

(1) $t \in (t_0, t_1)$, the control remains on its upper bound $u^*(t) = 100$
(2) $t \in (t_1, t_2)$, the control remains on its lower bound $u^*(t) = 0$
(3) $t \in (t_2, t_f)$, the control is constant

The optimal control profile is obtained by computing the switching times t_1 and t_2, and the constant control.

6.4 Simulation Results

In order to simulate real behaviour of the process, the valve constants are perturbed to following values: $k_{11} = 10.08\,\mathrm{cm}^{2.5}\,\mathrm{s}^{-1}$ and $k_{22} = 8.82\,\mathrm{cm}^{2.5}\,\mathrm{s}^{-1}$. The initial conditions remain unchanged. The measured outputs are states with addition of white noise. It is also considered that full-time measurements are available. While the NE controller is designed using the nominal mathematical model, the simulations are performed for measured outputs from the perturbed model. Difference between nominal and perturbed model causes variations which in turn result in a performance loss and terminal constraint violation, when applying the open-loop control profile (see Figure 5). Run-to-run constraint adaptation is initialised with a constraint bias of $\delta\psi = 0$ and considers a filter gain of $W = 0.5$. For proposed integrated control scheme a filter gain was set to $W = 0.4$. The filter parameters were chosen as a compromise between a controller aggressiveness and an ability to deal with measurement noise.

Figure 6 compares the evolution of the performance during the first 15 runs. The evolution of the terminal constraint is presented in the left plot. See that in the first run pure constraint adaptation starts far from the desired value compared to the neighbouring extremal approach. In the consequent runs, the constraints remains inactive with the pure neighbouring extremal approach. In contrast, with pure constraint adaptation and with integrated two-time-scale scheme, the terminal constraint is enhanced over the runs to meet the goal. The pure constraint adaptation approach needed 5 runs to converge. Then, in last 10 runs approach oscillates around the desired value. Note that this approach seems to be more sensitive to measurement noise then the other approaches because only end-point measurement is considered. The integrated scheme starts in close proximity of terminal constraint. In the following runs, this result is slowly enhanced to meet the terminal constraint. Due to the fact that control corrections are applied during each run as well, this approach is able to correct the control profile with lower sensitivity to measurement noise. These corrections affects also the end-point measurement which is less variant over the runs. Note that the sensitivity of NE controller to measurement noise is relative to the chosen number of NE corrections. Lower number expresses lower noise sensitivity but worse corrections and vice versa. In this case study, 120 NE corrections have been chosen.

The right plot of Figure 6 shows the evolution of the modelled terminal constraint hence the original terminal constraint plus constraint bias. This value varies a little for the integrated scheme because the NE controller in the inner loop is able to recover a large portion of optimality loss. In contrast, constraint adaptation requires heavier adaptation since no correction is made during the run.

The resulting control profile after adaptation within 15 runs is shown in left plot in Figure 7. The optimal control profile still consists of the tree arcs, but the switching times have changed compared to nominal solution displayed in Figure 5, as a result of the constrained adaptation. The corresponding measured levels are presented in the right plot in Figure 7. It can be seen that the measured level in second tank met the desired level with proposed integrated two-time-scale control approach.

6.5 Experimental Results

The nominal solution was obtained for certain positions of outflow valves (leakages). In order to test the performance of the control approaches, the outflow was increased. This change also invoked minor variation of initial conditions. Measurements of levels were available on-line, as required. The conversion between measured outputs (in volts) and

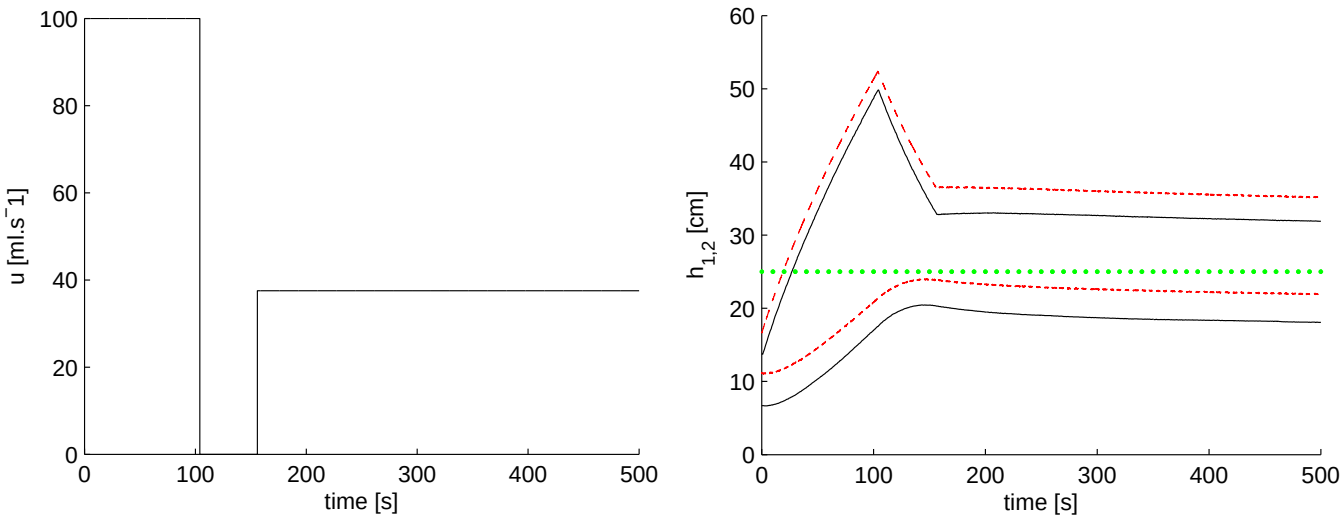

Fig. 5. **Left:** Nominal control trajectory; **Right:** Response for open-loop implementation of nominal control trajectory, **solid line:** nominal model, **dashed line:** perturbed model, and **bold dotted line:** desired level in the second tank.

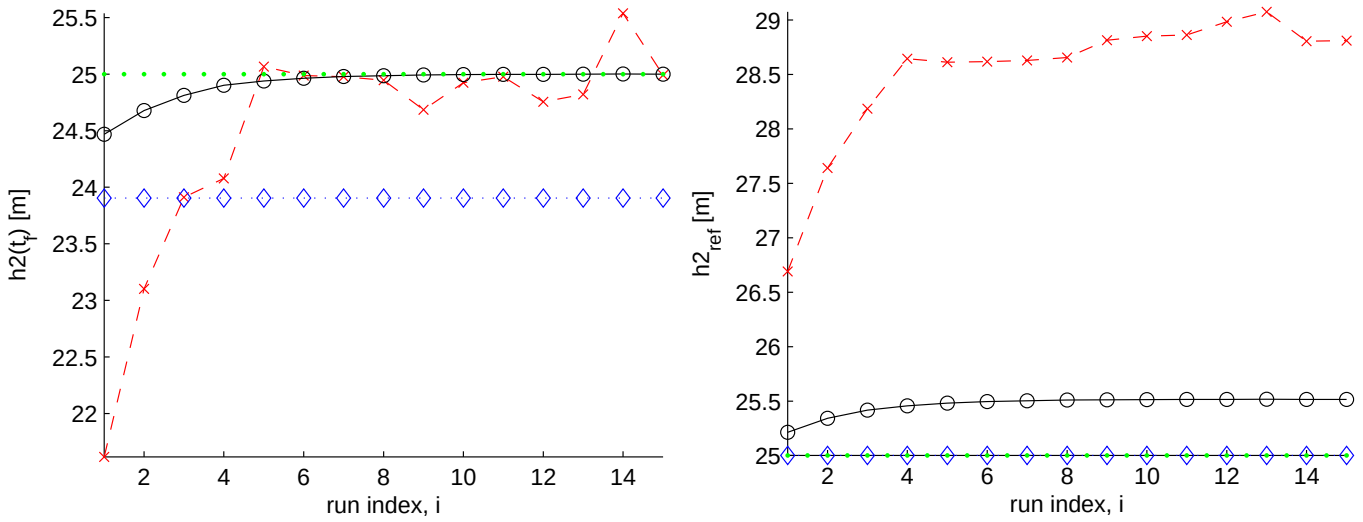

Fig. 6. Control approaches in simulations. **Dashed line with crosses**: pure constraint adaptation, **dotted line with diamonds**: pure neighbouring extremal control, **solid line with circles**: integrated two-time-scale scheme control, **bold dotted line:** desired level. **Left plot**: Evolution of the measured terminal constraint; **Right plot**: Evolution of the modelled terminal constraint.

states (in centimetres) was considered as another perturbation. As in simulations, the difference between model and process is causing performance loss and terminal constraint violation. Run-to-run constraint adaptation is initialised with a constraint bias of $\delta\psi = 0$ and considers a filter gain of $W = 0.6$. For proposed integrated control scheme a filter gain was set to $W = 0.5$. As previously, the filter parameters were chosen with respect to measurement noise and controller dynamics. Sampling time was set to 2 ms as the highest time instant needed to redesign NE controller. In order to reduce the sampling time, the design of NE controller starts an instant before second switching time as there are no control corrections along boundary arc.

Performance evolution over 15 runs of stand-alone approach and proposed two-time-scale approach is displayed in Figure 8. Left plot shows the development of terminal constraint. Similar results as in simulations can be observed. In the first run, NE and proposed two-time-scale approach start closely to the desired value. NE controller is able to recover some of performance loss but not completely. In consequent runs, two-time-scale slowly augments terminal constraint of model to satisfy the objective. In this case, first 3 runs were needed to almost reach the optimum. In last 9 runs, terminal constraint holds closely to desired level value and can be considered as active. The performance of NE does not change as control updates are only carried within the run and not between them as in case of two-time-scale and pure constraint adaptation. In contrast to proposed approach, pure run-to-run adaptation of constraints needed first 6 runs to come close to optimum but with higher value of filter gain. In the following runs, terminal constraint values oscillates around desired level value. This approach is more sensitive to

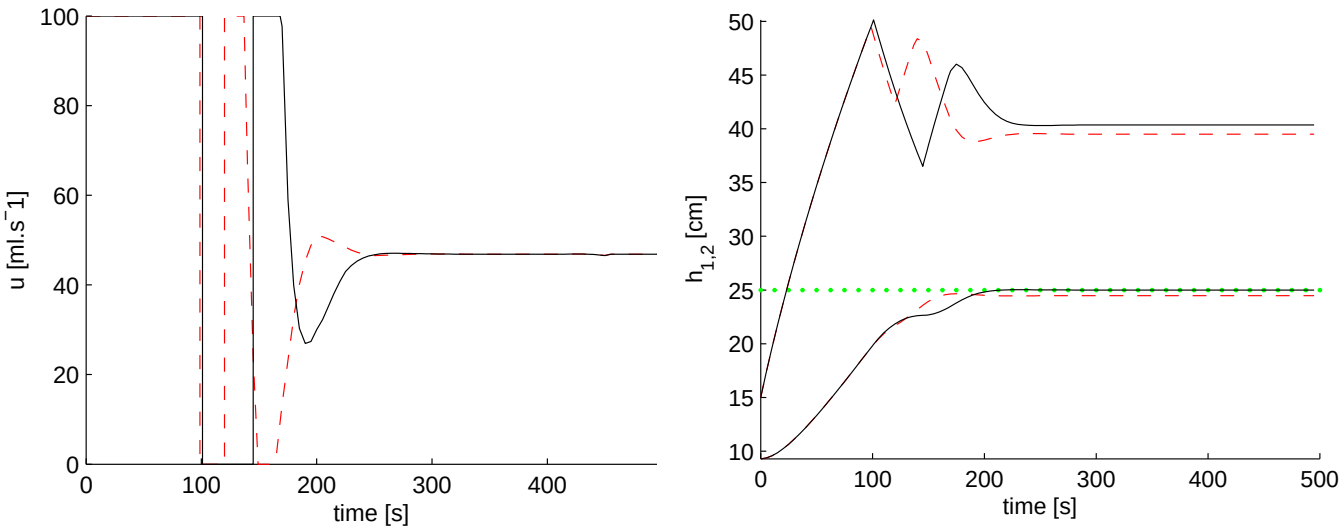

Fig. 7. Performance of proposed scheme in simulations with perturbed valve constants after 1st and 15th run of adaptation. **Left plot**: Control trajectory; **Right plot**: Measured outputs; **Dashed line**: First run; **Solid line**: Last run; **Bold dotted line**: Desired level.

measurement noise in comparison to the other approaches as only final measurements are taken. Proposed two-time-scale approach is able to correct the control profile with lower sensitivity to measurement noise, due to the fact that control corrections are applied during each run as well. This also results in more equal end-point measurements. In experiment, 750 NE corrections were performed. This higher number of NE updates caused high frequency noise in control actions. Thus, these inputs were filtered on-line in order to deliver smoother control actions.

Terminal constraint evolution plus constraint bias is depicted in the right plot of Figure 8. Observe small variations of this value for proposed scheme. In-run control corrections by NE controller provided more equal performance. Since no correction is made during the run, pure constraint adaptation approach clearly requires heavier adaptation.

Left plot in Figure 9 displays the resulting control profile after adaptation within 15 runs. The suboptimal control profile still begins with two boundary arcs but the switching times have changed compared to nominal solution displayed in Figure 5, as a result of the constrained adaptation. The unconstrained arc is no longer constant as is corrected by NE controller. Note that large state variations may cause unproportional control correction what results into clipped control. Right plot in Figure 9 presents corresponding measured levels. Obviously, the measured level in second tank meets the desired level with proposed integrated two-time-scale control approach.

7. CONCLUSIONS

In this paper, an integrated two-times-scale control scheme for level control of two connected tanks has been proposed. Simulation and experimental results show that this control approach improves the performance of dynamic real-time optimisation applied to the real process. The combination of two approaches, namely run-to-run adaptation and neighbouring extremal control, allows to complement the benefits of each other while mitigating some of their deficiencies. Standalone implementation of these approaches indicates lower performance compared to proposed approach. On one side, the NE approach can improve performance loss within the run, and on the other side, constraint adaptation handles terminal constraints. Advantages of the integrated scheme have been demonstrated on the case study for level control of two connected tanks with liquid interaction. As part of future work, an extension of the current scheme to singular control problems is currently under investigation, as well as the ability to handle problems with state path constraints.

ACKNOWLEDGMENTS

The authors gratefully acknowledge the contribution of the Scientific Grant Agency of the Slovak Republic under the grant 1/0071/09. Also supported by a grant (No. NIL-I-007-d) from Iceland, Liechtenstein and Norway through the EEA Financial Mechanism and the Norwegian Financial Mechanism. This project is also co-financed from the state budget of the Slovak Republic.

This contribution/publication is the partial result of the R&D Operational Programme for the project Support of Center of Excellence for Smart Technologies, Systems and Services, ITMS 26240120005, co-funded by the ERDF.

REFERENCES

Allgöwer, F. and Zheng, A. (2000). *Nonlinear Model Predictive Control*. Birkhäuser Verlag.

Bemporad, A., Morari, M., Dua, V., and Pistikopoulos, E.N. (2002). The explicit linear quadratic regulator for constrained systems. *Automatica*, 38(1), 3–20.

Biegler, L. (2000). Efficient solution of dynamic optimization and nmpc problems. *Nonlinear Model Predictive Control*, 219–244.

Bonvin, D., Srinivasan, B., and Hunkeler, D. (2006). Control and optimization of batch processes: Improvement of process operation in the production of specialty chemicals. *IEEE Control Systems Magazine*, 26(6), 34–45.

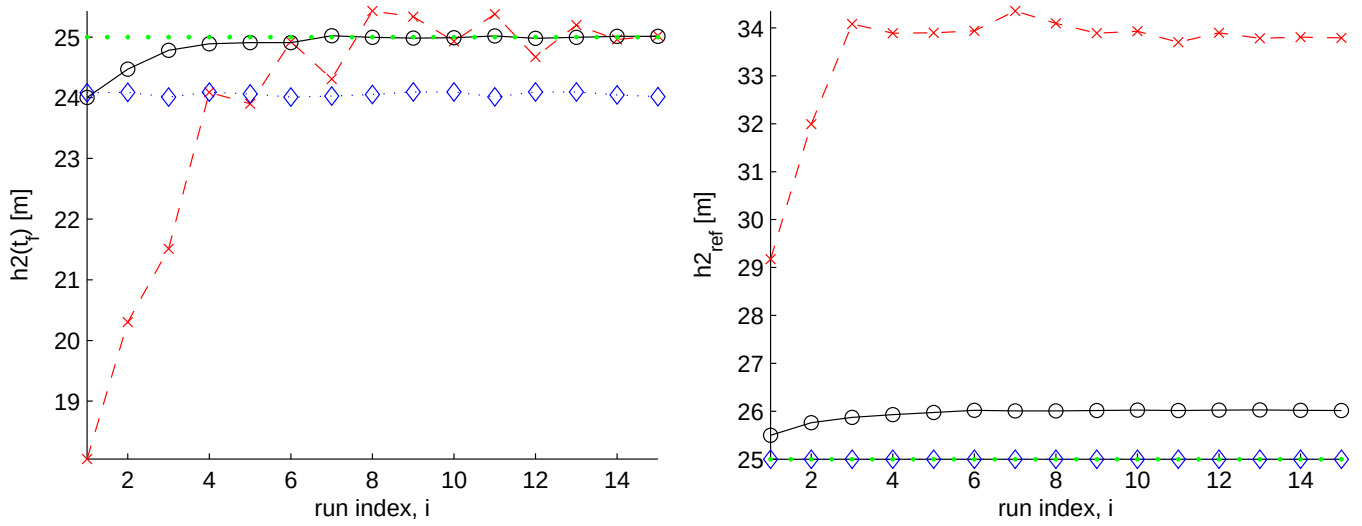

Fig. 8. Control approaches in real conditions. **Dashed line with crosses**: pure constraint adaptation, **dotted line with diamonds**: pure neighbouring extremal control, **solid line with circles**: integrated two-time-scale scheme control, **bold dotted line:** desired level. **Left plot**: Evolution of the measured terminal constraint; **Right plot**: Evolution of the modelled terminal constraint.

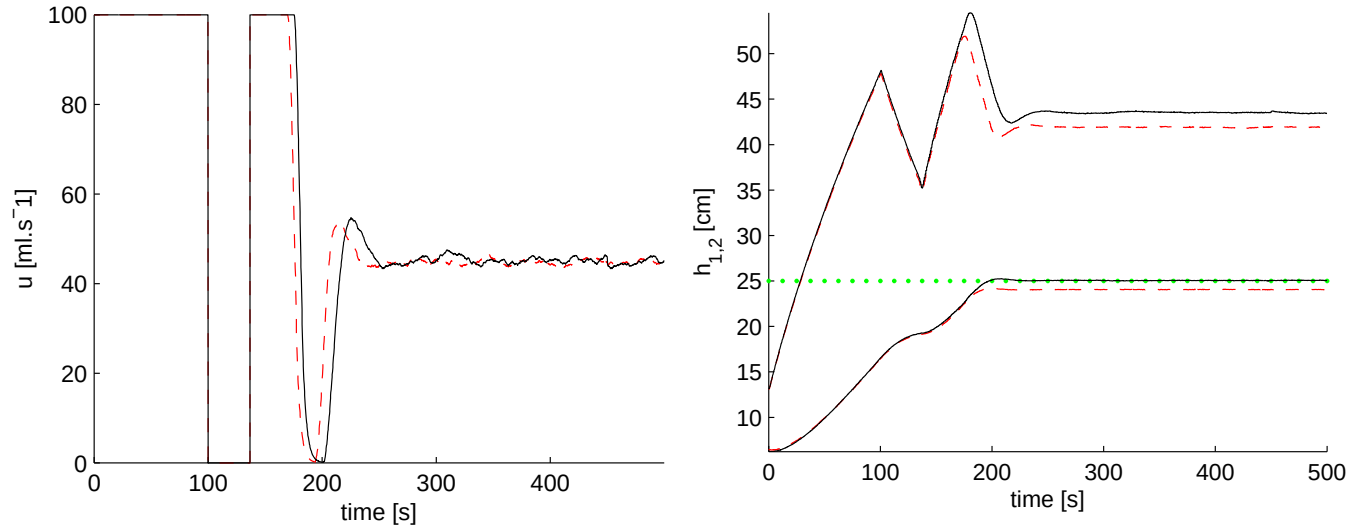

Fig. 9. Experimental performance of proposed scheme after 1st and 15th run of adaptation. **Left plot**: Control trajectory; **Right plot**: Measured outputs; **Dashed line**: First run; **Solid line**: Last run; **Bold dotted line**: Desired level.

Bryson, A.E. and Ho, Y.C. (1975). *Applied Optimal Control – Optimization, Estimation and Control*. Hemisphere publishing corporation.

Cannon, M., Kouvaritakis, B., Lee, Y.I., and brooms, A.C. (2001). Efficient non-linear model based predictive control. *International Journal of Control*.

Diehl, M., Findeisen, R., Nagy, Z., Bock, H.G., Schlöder, J.P., and Allgöwer, F. (2002). Real-time optimization and nonlinear model predictive control of processes governed by differential algebraic equations. *Jour. of Process Control*.

Edgar, T.F. and Himmelblau, D.M. (1988). *Optimization of Chemical Processes*. McGraw-Hill, New York.

Garcia, C.E., Prett, D.M., and Morari, M. (1989). Model Predictive Control: Theory and Practice – A Survey. *Automatica*, 25(3), 335–348.

Guntern, C., Keller, A., and Hungerbuhler, K. (1998). Economic Optimization of an Industrial Semi-batch Reactor Applying Dynamic Programming. *Industrial and Engineering Chemistry Research*, 37(10), 4017–4022.

Kadam, J.V. and Marquardt, W. (2007). Integration of economical optimization and control for intentionally transient process operation. *Lecture Notes in Control and Information Sciences*, 358, 419–434.

Maciejowski, J.M. (2002). *Predictive Control with Constraints*. Prentice-Hall, London.

Marchetti, A., Chachuat, B., and Bonvin, D. (2007). Batch process optimization via run-to-run constraints adaptation. In *European Control Conference*. Kos, Greece.

Pesch, H.J. (1989). Real-time computation of feedback controls for constrained optimal control problems. Part II: A correction method based on multiple shooting. *Optimal Control Applications & Methods*, 10, 147–171.